

## Raman spectroscopy of graphitic foams

E. B. Barros,<sup>1,5,\*</sup> N. S. Demir,<sup>2</sup> A. G. Souza Filho,<sup>1</sup> J. Mendes Filho,<sup>1</sup> A. Jorio,<sup>3</sup> G. Dresselhaus,<sup>4</sup> and M. S. Dresselhaus<sup>2,5</sup><sup>1</sup>Departamento de Física, Universidade Federal do Ceará, Fortaleza, Ceará, 60455-760, Brazil<sup>2</sup>Department of Physics, Massachusetts Institute of Technology, Cambridge, Massachusetts 02139-4307, USA<sup>3</sup>Departamento de Física, Universidade Federal de Minas Gerais, Belo Horizonte, MG, 30123-970, Brazil<sup>4</sup>Francis Bitter Magnet Laboratory, Massachusetts Institute of Technology, Cambridge, Massachusetts 02139-4307, USA<sup>5</sup>Department of Electrical Engineering and Computer Science, Massachusetts Institute of Technology,

Cambridge, Massachusetts 02139-4307, USA

(Received 23 October 2004; published 18 April 2005)

The recently developed pitch-based graphitic foams have a very high thermal conductivity to weight ratio. This property allows graphitic foams to be used in several thermal management applications, especially in the aeronautics and aerospace industries. Raman spectroscopy studies were performed on the different structural regions of the foam, yielding important information on the structural properties of the graphitic foams, as well as on the physical properties of graphite. The graphitic foam was found to be composed of two intermixed graphitic structures, one with stacked planes and one with a turbostratic structure. This special structure allowed for a simultaneous study of the properties of two-dimensional (2D) and three-dimensional (3D) graphitic structures. The dispersion of the  $G'$  band was found to be different for 2D and 3D graphite. The intensity of the  $D$ -band Raman feature was used to probe the density of defects in the structure, leading to the conclusion that the defects are mainly localized in the 2D structures. A simple model is proposed to explain the origin of the two different structures within the graphitic foam. Also, the dependence of the  $G'$  band on polarization is addressed.

DOI: 10.1103/PhysRevB.71.165422

PACS number(s): 78.30.Hv, 61.43.Gt, 78.30.Ly

## I. INTRODUCTION

The recent development of a pitch-based graphitic foam obtained through the graphitization of carbon foams has attracted attention due to its potential for use in low-density thermal management devices.<sup>1</sup> This graphitic foam is characterized by highly aligned graphitic structures around the host spherical cells. With a very high thermal conductivity to weight ratio, graphitic foam is a promising material for applications, particularly in utilizing the high specific thermal conductivity in the aeronautics and aerospace industries. Despite the many studies<sup>1-5</sup> of the properties of these porous carbon materials, the heat transfer processes that allow for such a high thermal conductivity are still not well understood.

Mesophase pitch-based graphitic foams represent a porous medium where the junctions between cells are distributed in a tetrahedral pattern. The structure of the graphitic foams can be described in terms of a regular assembly of spherical cells surrounded by graphitic material, forming a regular tetrahedron of graphitic material with a cell associated with each of its vertices. The spherical cells intersect with each other forming pores of various sizes. The relation between the size of the tetrahedron and the radius of the cells determines the porosity of the medium.<sup>3</sup> Figure 1(a) shows an illustrative diagram of two junctions calculated for two different porosities (78% and 98%), defined as the ratio between the cell volume to the total volume.<sup>3</sup> These tetrahedral junctions are then interconnected to form the carbon foam. Each junction is connected through ligaments to four other junctions in the directions of a regular tetrahedron. In the illustration of the foam with 98% porosity shown in Fig. 1(a), the ligaments are easily seen as the four ends connected

to the center of the junction. For porosities less than 78%, the ligaments are not easily observed, because they become thick

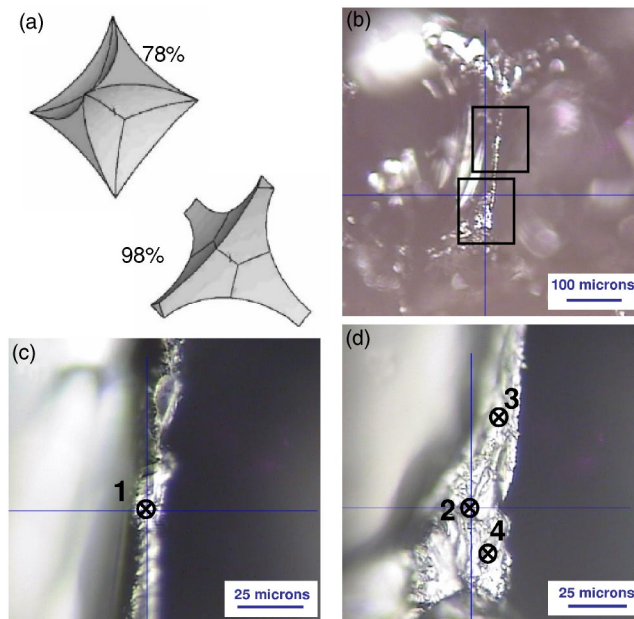


FIG. 1. (a) Illustrative diagrams of two junctions of a graphitic foam, one for 78% porosity and the other for 98% porosity. (b) Optical image of the graphitic foam showing an overall view of the porous structure of the foam. The squares show the areas of the graphitic foam where the Raman spectra were obtained. Higher magnification images of the upper and lower squared regions are shown in (c) and (d), respectively. The numbers indicate the center of the laser spot for each Raman spectrum presented in the text.

and are more like the junction itself. It is clear that the difference between the properties of the ligaments and the junction should become less evident for lower porosity foams.

According to findings from x-ray analysis, the average interplanar spacing of the (002) graphitic planes for the graphitic foam is  $d_{002}=3.355$  Å, corresponding to the average interlayer spacing of graphite. Stack heights were found to be as large as  $\sim 80$  nm, with crystallite sizes of up to approximately 20 nm.<sup>2</sup> Furthermore, thermal conductivity ( $\kappa$ ) measurements indicate that  $\kappa$  for the resulting graphitic foams ranges from 40 to 150 W/mK.<sup>1</sup> Considering the thermal conductivity to weight ratio, the specific thermal conductivity of graphitic foams is about 4 to 5 times higher than that of copper and about 2 times higher than the specific thermal conductivity of graphite.<sup>1</sup>

Previous high resolution TEM and optical studies with polarized light<sup>2</sup> have shown that the ligaments are usually highly oriented and defect-free graphitic lattices, with the graphitic planes oriented parallel to the ligament axis. However, in the region of the junctions, a great number of defects are found, as the differently oriented graphitic layers from different ligaments come together.

The heat transfer in solids is mainly governed by the properties of phonon propagation. Therefore the use of Raman spectroscopy should be of great use for the characterization of the graphitic foams. The very unique Raman spectra of graphite normally consists of mainly three strong features. The  $G$  band, with a characteristic frequency of  $1582\text{ cm}^{-1}$ , is observed in single crystal graphite and corresponds to the in-plane vibrations of the nearest neighbor atoms in the graphene (2D graphite) layers. The other two commonly observed features, known as the  $D$  and  $G'$  bands, both originate from a  $q \neq 0$  phonon near the Brillouin zone boundary through a double resonance process.<sup>6,7</sup> It has been shown that the process responsible for the  $D$  band depends on the presence of lattice defects.<sup>6,8</sup> Therefore, it is expected that the intensity of the  $D$  band relative to the  $G$  band can be used to probe the distribution of defects in any  $sp^2$  carbon-based system. The  $G'$  band originates from a second-order scattering process involving  $+q$  and  $-q$  phonons, and, though its occurrence does not depend on defects, its frequency is given by  $\omega_{G'} \sim 2\omega_D$ , where  $\omega_D$  denotes the  $D$  band frequency.<sup>9,10</sup> The  $G'$  band of an isolated graphene layer (2D graphite) is different from that of bulk graphite, where the ...ABAB... stacking of the graphene layers is believed to cause a splitting in the graphite Raman feature related to the  $G'$  band. The dispersion of the single peak  $G'$  band feature of 2D graphite can be obtained from the work of Cançado *et al.*<sup>8</sup> on turbostratic graphite and is found to be  $\sim 106\text{ cm}^{-1}/\text{eV}$ . For 3D graphite, the frequency of the strongest peak and an approximate value for its dispersion can be obtained from the work of Matthews *et al.*<sup>11</sup> on highly oriented pyrolytic graphite (HOPG). For an excitation of 2.41 eV, the frequency of the strong  $G'$  band peak was found to be approximately  $2726\text{ cm}^{-1}$  with a dispersion of  $\sim 94\text{ cm}^{-1}/\text{eV}$ . The study of the dispersion of the double peak structure of 3D graphite is still in an early stage and the physical reason for the difference in the dispersion for 2D and 3D graphite is still unexplained in the literature. Only a few values for the frequency and the dispersion of the

weaker peak on the  $G'$  band of 3D graphite could be obtained from the literature.<sup>12</sup>

In this work we show the analysis of a set of Raman scattering experiments performed on different structural regions of a graphitic foam. Raman spectroscopy was found to provide a powerful tool to study the structural properties of these carbon-based systems. The Raman spectra analysis was successful in differentiating between the contributions from the two limiting cases of interplane interaction, highly aligned graphitic regions where the planes show stacking order and the structural behavior follows that of HOPG (3D), and poorly aligned graphitic regions where the decrease in the interplane interaction causes the structural behavior to approximate that of isolated graphene (2D) layers. For that reason, the graphitic foam material could be used to provide important information on the contrasting properties of 2D and 3D graphite, such as the thermal conductivity and the vibrational properties. In this way, the difference in the processes responsible for the  $D$  and  $G'$  bands of 2D and 3D graphitic layers could be addressed by studying the Raman spectra of graphitic foams.

## II. EXPERIMENT

The graphitic foam samples in this study were prepared at Oak Ridge National Laboratory (ORNL) using Mitsubishi ARA24 Mesophase pitch. The synthesis procedure begins with carbonizing and pyrolyzing a mesophase pitch at  $1000\text{ }^\circ\text{C}$ , and graphitizing the resulting material at  $2800\text{ }^\circ\text{C}$ . The graphitization heating rate was of  $0.5\text{ }^\circ\text{C}/\text{min}$ . The resulting material was then cut into small cubic samples with 1.5 cm on a side. Previous studies showed that the properties of the graphitic foam depend strongly on the graphitization heating rate used on its preparation. For heating rates varying between  $0.5\text{ }^\circ\text{C}/\text{min}$  and  $1.5\text{ }^\circ\text{C}/\text{min}$ , the resulting densities of the foams ranged from  $0.2\text{--}0.6\text{ g}/\text{cm}^3$ , and the average diameters of the pores were within the range of  $275\text{--}350\text{ }\mu\text{m}$  for the ARA24-derived foams used in the present study.<sup>1</sup>

The Raman spectroscopy experiments were performed using 1.58 eV excitation from a Ti:sapphire laser and 2.41 eV excitation from an argon ion laser. A  $50\times$  objective was used to focus the laser beam on the sample, resulting in a laser spot of about  $3\text{ }\mu\text{m}$ . The back scattering geometry was applied with the use of two polarizers in the laser pathway for the incident and the scattered light. For simplicity, only two polarization geometries were used, with both the incident and scattered light polarized either along the horizontal (HH) or along the vertical (VV) directions of Figs. 1(b)–1(d).

## III. RESULTS AND DISCUSSION

Figure 1(b) shows an optical image of the region of the sample studied here. This picture was taken using a low magnification lens ( $10\times$ ), and it shows the porous structure of the graphitic foam, giving an overall image of the region where the experiment was performed. Throughout the process of cutting the sample into small cubes, several junctions and ligaments were sectioned so that they could be observed from the outer surface of the sample. By studying these sec-

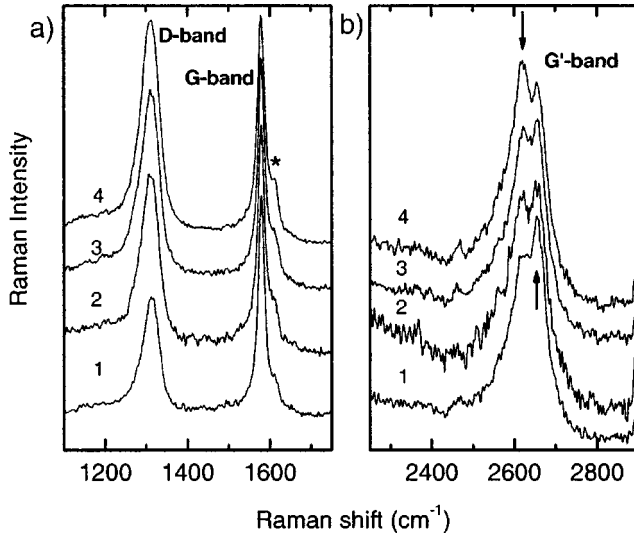


FIG. 2. Raman spectra taken on different regions of the graphitic foam in Figs. 1(c) and 1(d) for the spectral region of (a) the  $D$  and  $G$  band and (b) the  $G'$  band. The Raman spectra in (a) and (b) were normalized to the intensity of the peaks at  $1582\text{ cm}^{-1}$  and  $2656\text{ cm}^{-1}$ , respectively. The asterisk marks the  $D'$  feature.

tioned areas, it is possible to probe the properties of the core of the graphitic structure instead of being limited to studying only its surface. Figures 1(c) and 1(d) show images of the sectioned region of the graphitic foam studied here taken at the region of the sample where the Raman experiment was performed and using the same  $50\times$  objective lens that was used to focus the laser beam. The numbers on Figs. 1(c) and 1(d) indicate the spots where the laser was focused to obtain the Raman spectra discussed below.

Figure 2(a) shows the  $D$  and  $G$  band Raman spectra obtained at different points (indicated by numbers 1, 2, 3, and 4 in Figs. 1 and 2) of the carbon foam sample. The spectra were taken with both the incident and scattered light polarized along the HH direction. The  $1.58\text{ eV}$  laser excitation energy was chosen because it is well known that the  $D$  band is usually stronger for red light excitation, and thus, it becomes easier to observe the changes in the  $D$  band intensity relative to the concentration of defects. The spectra in Fig. 2(a) were all normalized to the intensity of the  $G$  band peak. Note that the  $D$  band intensity is enhanced relative to that of the  $G$  band when moving from spots 1 to 4. It is clear that the concentration of defects is lowest in the spot labelled 1 on Fig. 1(c). It should also be mentioned that the process of cutting the graphitic foam is likely to increase the level of disorder in the ligaments and junctions. However, the difference in the  $D$  band intensity observed for the various spots

(see Figs. 1 and 2) is likely to be mainly due to differences in the original disorder within the graphitic structure. The intensity of the small feature, known as the  $D'$  band, observed at a frequency slightly higher than that of the  $G$  band ( $\sim 1620\text{ cm}^{-1}$  and marked with an asterisk) follows the behavior of the  $D$  band intensity. The  $D'$  band feature is also associated with the presence of defects in the lattice and originates from a double resonance process involving  $q \sim 2k$  phonons close to the Brillouin zone center ( $\Gamma$  point intervalley process<sup>7,13</sup>).

Figure 2(b) shows the Raman spectra of the  $G'$  band for the same four spots as in Fig. 1(c). The intensity was normalized relative to the intensity of the peak at  $2656\text{ cm}^{-1}$ . Based on previous studies of the  $G'$  band of PPP (Ref. 8) and HOPG,<sup>11</sup> the peak at approximately  $2619\text{ cm}^{-1}$  (down arrow) could be assigned to contributions from 2D graphite present in the sample, while the peak at  $2656\text{ cm}^{-1}$  (up arrow) comes from the contribution of highly aligned 3D graphitic structures. It is clear that the frequency of the  $G'$  should change with different interplanar distances. Therefore we should interpret the  $G'(2D)$  and  $G'(3D)$  peaks observed here as the two limiting cases, while the intermediate cases with the interplanar distance between that of ideal 3D graphite and 2D turbostratic graphite give rise to a line broadening of these peaks. The same broadening effect is observed for the  $D$  band peak. For this reason, the 2D and 3D components of the  $D$  band could not be resolved. As seen in Fig. 2(b), the lower frequency [ $G'(2D)$ ] peak evolves from a low intensity shoulder to a strong peak, when the position of the light beam on the sample is changed from the spots 1 to 4. By comparing Figs. 2(a) and 2(b), it is possible to see a correlation between the relative intensities  $I_D/I_G$  and  $I_{G'(2D)}/I_{G'(3D)}$  at the four locations on the sample. It is important to mention that for some regions of the sample this correlation did not appear to be as clear (not shown here) as in the data shown in Fig. 2.

The Raman spectra obtained in this experiment were decomposed into a set of Lorentzian peaks. For simplicity, the  $D$  band was considered to be composed of a single peak while the  $G'$  band was considered to be composed of four peaks in accordance with the following physical identification: one with a frequency of around  $2468\text{ cm}^{-1}$  which corresponds to the  $K$  point phonon modes,<sup>7</sup> and three peaks in the range between  $2550$  and  $2680\text{ cm}^{-1}$ , one corresponding to the contribution from 2D graphite [ $G'(2D)$ ] and two from the 3D graphite regions [ $G'(3D)_1$  and  $G'(3D)_2$ ]. A good fit to the experiments was obtained by using this approach, and the frequencies obtained for the best fit are listed in Table I. Also, in Table I, the fitting values obtained by using  $2.41\text{ eV}$  laser excitation are shown, for comparison. It was also observed that for  $1.58\text{ eV}$  ( $2.41\text{ eV}$ ) excitation energy, the line-

TABLE I. Raman frequencies (in  $\text{cm}^{-1}$ ) for the  $D$  and  $G'$  bands of the graphitic foams. The error in the  $G'(3D)_1$  frequency value is very large due to the low intensity of this peak compared to that of the other  $G'$  components.

$E_{\text{Laser}}$	$\omega_D$	$\omega_{G'(3D)_1}$	$\omega_{G'(2D)}$	$\omega_{G'(3D)_2}$
1.58 eV	$1312 \pm 3$	$2575 \pm 20$	$2619 \pm 4$	$2656 \pm 4$
2.41 eV	$1353 \pm 3$	$2676 \pm 20$	$2700 \pm 4$	$2728 \pm 4$

width of the  $G$  band is increased by 10% (20%) when the  $G'(2D)$  intensity is strong. In the light of previous work,<sup>14</sup> the increase in the linewidth is caused by the presence of two unresolved  $G$ -band peaks, one that originates from the 3D graphite and another one from the 2D graphite within the laser spot. Considering that the 2D graphite does not have a good heat sink, thus being more sensitive to the heating caused by the incidence of the laser beam than the 3D graphite, the incident laser will cause a small downshift in the frequency of the  $G$  band of the 2D graphite. Therefore, when the concentration of 2D graphite is high within the laser spot, the contribution of the 2D graphite to the  $G$  band is strong and a wider linewidth is observed for this Raman feature.

From Table I, it is possible to make an estimate of the dispersion of the  $D$  and  $G'$  bands. The dispersion of the  $G'(3D)_2$  peak ( $\sim 87 \text{ cm}^{-1}/\text{eV}$ ) is about 13% less than the dispersion of the  $G'(2D)$  band ( $\sim 99 \text{ cm}^{-1}/\text{eV}$ ). This result is in good agreement with previous studies for 2D graphite<sup>8</sup> and for 3D graphite.<sup>11</sup> Also, the average between the frequencies of the two  $G'(3D)$  peaks is  $\sim 2615.5 \text{ cm}^{-1}$  for the 1.58 eV excitation and  $\sim 2702 \text{ cm}^{-1}$  for the 2.41 eV excitation. These values are very close, within experimental error, to the frequencies of the  $G'(2D)$  peak, which are of  $2619 \text{ cm}^{-1}$  for the 1.58 eV excitation and  $2700 \text{ cm}^{-1}$  for the 2.41 eV excitation, which is consistent with the notion that the double peak structure observed for the  $G'$  feature of 3D graphite originates from a splitting of the  $G'$  phonon feature.

Note that both the frequency and the dispersion of the  $G'$  peak that originates from the 2D graphite within the optical beam are approximately 2 times those of the  $D$  band, while the frequency of the more intense  $G'$  peak for 3D graphite is higher by more than  $20 \text{ cm}^{-1}$  (see Table I) and the dispersion is less than 2 times the dispersion of the  $D$  band. This result suggests that the strong  $D$ -band feature also originates from 2D graphite and not from the highly aligned (3D) graphitic regions of the foam. The small difference between the frequency of the  $G'(2D)$  feature and 2 times the frequency of the  $D$  band arises from the fact that only one peak is being considered for the  $D$  band. The frequency difference of approximately  $5 \text{ cm}^{-1}$  observed here is in good agreement with the work of Cançado *et al.*,<sup>8</sup> where it is shown that the  $D$ -band feature is composed of two peaks separated by approximately  $9 \text{ cm}^{-1}$  and that, for a Stokes process, the frequency of the  $G'$  peak is 2 times the frequency of the lower  $D$  peak. It should be noted that in regions where the  $D$ -band intensity is weak, the intensity of the  $D$ -band changes from point to point [as shown in Figs. 2(a) and 2(b)], but the frequency and the line shape of the  $D$  band remain mostly unchanged. Consequently, it can be understood that the main contribution to the disorder-induced peaks comes from the unaligned graphite (2D) present in the sample. Therefore, we conclude that the concentration of defects in the aligned 3D graphite within the light beam should be low.

The two-dimensional behavior observed for some regions of this sample is very similar to that observed in turbostratic graphite structures.<sup>8</sup> In those structures, the graphene planes are not stacked with respect to one another with the ...*ABAB*... structure. Therefore the distance between the planes is increased, thus weakening the interaction between the graphene layers, causing the planes to behave as if they

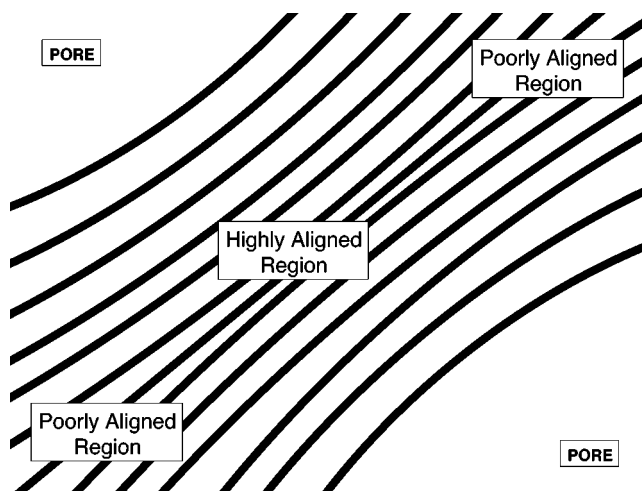


FIG. 3. Illustrative model showing how the graphene planes are displaced in graphitic foams. This simple model explains the main process responsible for the 2D and 3D graphitic regions observed in the graphitic foam sample.

were isolated. In the case of the graphitic foams, 2D graphite regions naturally originate from the fact that the curvature of the cell walls must be followed by the surrounding graphitic planes. Figure 3 shows an illustrative diagram of a simple model that explains the main process responsible for the presence of both 2D and 3D graphite regions in the graphitic foam. Also, scanning electron microscopy studies have shown the presence of highly curved and folded graphitic planes within the region of the junction of the ligaments.<sup>2</sup> These highly curved regions should also have a turbostratic structure.

Figure 4 shows the Raman spectra taken at position 1 of Fig. 1(c) for two different polarization geometries, as depicted in the inset of Fig. 4. The absolute Raman intensities

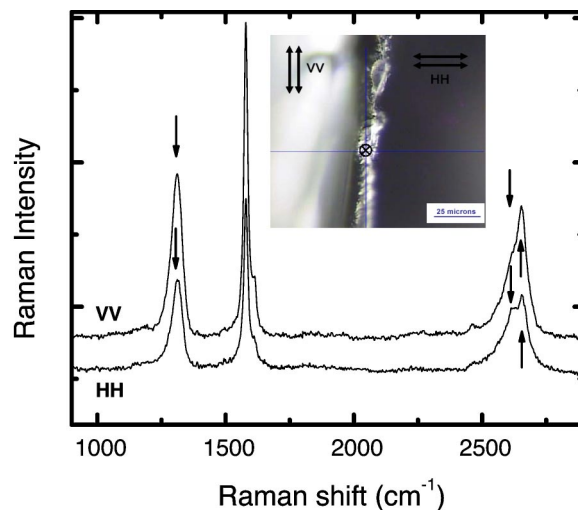


FIG. 4. Raman spectra taken with two different geometries in the region 1 of Fig. 1(c). The HH geometry had incident and scattered light polarized perpendicularly to the ligament axis while the VV geometry has light polarized in parallel to the ligament axis. The inset to the figure depicts the different scattering geometries.

are plotted in this figure. As can be observed, the peaks for the VV polarization configuration are much stronger than those for the HH polarization. It is well known that the Raman intensity for light polarized along the direction of the graphitic planes can be up to 4 times stronger than that for light polarized perpendicular to the planes.<sup>15</sup> Therefore, this polarization dependence suggests that the planes are well aligned with the vertical direction of Fig. 1(c), which is in agreement with the usual description of the graphitic foam based on transmission electron microscopy (TEM) measurements,<sup>2</sup> where it has been shown that the graphene planes are oriented along the ligaments. An interesting effect is observed for the  $G'$ -band spectra. The line shape of the  $G'$  band changes drastically with the change in the polarization geometry. This effect is a result of the fact that the intensity of the middle frequency peak (at  $2616\text{ cm}^{-1}$ ), which originates from the 2D region of the material, changes very little with the polarization. In fact, the intensity of this peak falls by only 20% when going from the VV to the HH polarization, while the intensity of the other peaks falls by approximately 50%. This result suggests that part of the 2D graphite present in this region is randomly oriented, and therefore its contribution to the Raman scattering does not depend strongly on the polarization geometry. Although there should be some aligned 2D graphite and some 3D graphite with defects in this region, it is clear that when the spectrum shows polarization independent behavior, it is mostly related to the 2D structure rather than the 3D structure.

#### IV. CONCLUSION

In summary, we have shown through Raman scattering experiments that the graphitic foam is composed of a mixture

of highly oriented graphitic structures with very good alignment between the graphitic planes, allowing ...*ABAB*... stacking to occur, and regions where the graphitic planes are not well aligned so that this turbostratic material behaves mainly like a 2D graphite. Also, the fact that the strong  $D$ -band peak corresponds to the unaligned 2D graphite suggests that the defects in the structure are concentrated in the unaligned regions of the material. Analysis of the  $D$ -band frequency and dispersion suggests that the contribution from the aligned graphite to the  $D$  band is small, and this corroborates the large magnitude of the observed thermal conductivity,<sup>1</sup> since the low concentration of defects allows a clear path for phonon propagation, thereby improving the heat transfer process. Furthermore the polarized Raman spectroscopy study shows that the polarization dependence of the  $D$  band and of the  $G'$  band do not follow the same pattern, thus yielding valuable structural information.

#### ACKNOWLEDGMENTS

The authors would like to thank Dr. J. Klett from the Oak Ridge National Laboratory for providing the samples and for his careful reading of the paper. The authors acknowledge support under NSF Grant No. DMR04-05538 and from a grant from the Intel Corporation. E.B.B. and A.G.S.F. acknowledge financial support from FUNCAP-Brazil, CNPq-Brazil (Grant No. 307417/2004-2), and CAPES-Brazil (PRODOC). A.J. acknowledges financial support from CNPq-Brazil. This work made use of MRSEC Shared Facilities at MIT supported by the National Science Foundation under Grant No. DMR-0213282 and NSF Laser Facility Grant No. CHE-011370.

\*Electronic address: ebarros@fisica.ufc.br

<sup>1</sup>J. Klett, R. Hardy, E. Romine, C. Walls, and T. Burchell, *Carbon* **38**, 953 (2000).

<sup>2</sup>J. W. Klett, A. D. McMillan, N. C. Gallego, and C. A. Walls, *J. Mater. Sci.* **39**, 3659 (2004).

<sup>3</sup>S. Sihn and A. K. Roy, *J. Mech. Phys. Solids* **52**, 167 (2004).

<sup>4</sup>Y. Kawashima and G. Katagiri, *Phys. Rev. B* **66**, 104109 (2002).

<sup>5</sup>S. M. Mukhopadhyay, N. Mahadev, P. Joshi, A. K. Roy, K. M. Kearns, and D. P. Anderson, *J. Appl. Phys.* **91**, 3415 (2002).

<sup>6</sup>C. Thomsen and S. Reich, *Phys. Rev. Lett.* **85**, 5214 (2000).

<sup>7</sup>R. Saito, A. Jorio, A. G. Souza Filho, G. Dresselhaus, M. S. Dresselhaus, and M. A. Pimenta, *Phys. Rev. Lett.* **88**, 027401 (2002).

<sup>8</sup>L. G. Cançado, M. A. Pimenta, R. Saito, A. Jorio, L. O. Ladeira, A. Grüneis, A. G. Souza Filho, G. Dresselhaus, and M. S.

Dresselhaus, *Phys. Rev. B* **66**, 035415 (2002).

<sup>9</sup>R. P. Vidano, D. B. Fishbach, L. J. Willis, and T. M. Loehr, *Solid State Commun.* **39**, 341 (1981).

<sup>10</sup>F. Tuinstra and J. L. Koenig, *J. Chem. Phys.* **53**, 1126 (1970).

<sup>11</sup>M. J. Matthews, M. A. Pimenta, G. Dresselhaus, M. S. Dresselhaus, and M. Endo, *Phys. Rev. B* **59**, R6585 (1999).

<sup>12</sup>P. H. Tan, Y. M. Deng, and Q. Zhao, *Phys. Rev. B* **58**, 5435 (1998).

<sup>13</sup>P. H. Tan, C. Y. Hu, J. Dong, W. Shen, and B. Zhang, *Phys. Rev. B* **64**, 214301 (2001).

<sup>14</sup>L. G. Cançado, M. A. Pimenta, B. R. A. Neves, G. Medeiros-Ribeiro, Toshiaki Enoki, Yousuke Kobayashi, Kazuyuki Takai, Ken-ichi Fukui, M. S. Dresselhaus, R. Saito, and A. Jorio, *Phys. Rev. Lett.* **93**, 047403 (2004).

<sup>15</sup>Y. Kawashima and G. Katagiri, *Phys. Rev. B* **59**, 62 (1999).